# A viable Labrador Sea rifting origin of the Northern

# 2 Appalachian and related seismic anomalies

- 3 Thomas Gernon<sup>1</sup>, Sascha Brune<sup>2,3</sup>, Thea Hincks<sup>1</sup> and Derek Keir<sup>1,4</sup>
- 4 <sup>1</sup> School of Ocean and Earth Science, University of Southampton, Southampton, UK
- 5 <sup>2</sup> GFZ Helmholtz Centre for Geosciences, Potsdam, Germany
- 6 <sup>3</sup> University of Potsdam, Potsdam-Golm, Germany
- <sup>4</sup> Dipartimento di Scienze della Terra, Universita degli Studi di Firenze, Florence, Italy

8

1

- 9 CITATION: Gernon, T., et al., 2025, A viable Labrador Sea rifting origin of the Northern
- 10 Appalachian and related seismic anomalies: Geology, v. XX, p. XXX–XXX,
- 11 | https://doi.org/10.1130/G53588.1

12

13

14

15

16

17

18

19

20

21

22

### **ABSTRACT**

The Northern Appalachian Anomaly is a prominent low seismic velocity zone, ~400 km in diameter, in the asthenosphere beneath New England. Previous studies interpret this shallow feature, occurring at a depth of ~200 km, as a thermal anomaly tied to edge-driven convection along the North American continental margins. Those studies recognize, however, that upwelling here is highly unusual since the passive margin has been tectonically quiescent for ~180 million years. We propose an alternative model, based on geologic observations, geotectonic reconstructions, and geodynamic simulations, that the anomaly instead represents a Rayleigh-Taylor instability linked to the breakup of the distant Labrador Sea continental margin. A Labrador Sea origin at breakup, ~85–80 Ma, would imply the migration of a chain of Rayleigh-Taylor

instabilities at a rate of ~22 km per million years, close to expected rates from geodynamic models. A migrating instability origin for the anomaly can reconcile its spatial characteristics, depth profile, and position near a long-inactive continental margin. A corollary is that the north-central Greenland anomaly, a mirror-image of the NAA, also potentially originated at the time of breakup. Further, the Central Appalachian Anomaly may fit this model if it represents an early-stage instability linked to rifting onset in the Labrador Sea. The Northern Appalachian Anomaly and other associated anomalies viably represent a legacy of continental rifting and breakup along the distant Labrador margins.

#### INTRODUCTION

The Northern Appalachian Anomaly (hereafter, NAA) is a contemporary thermal anomaly located in New England, centered beneath New Hampshire (Fig. 1A). The NAA is defined by the presence of low-degree partial melt interpreted to result from localized asthenospheric upwelling in response to edge-driven convection (Menke et al., 2016). Earthquake tomographic modeling suggests it is a slow seismic velocity anomaly at a depth of approximately 200 km (Menke et al., 2016; Schmandt and Lin, 2014; Pollitz and Mooney, 2016), or shallower (i.e., ~100 km; Brunsvik et al., 2024). Seismic models indicate that it is 350 to 400 km in diameter and elongated in a NE-SW or NNE-SSW direction (Fig. 1). The maximum shear velocity contrast at 200 km depth is up to ~4%, with a compressional-to-shear velocity perturbation ratio which is close to 1, supporting a thermal origin (Menke et al., 2016). This magnitude of anomaly likely corresponds to a ~100–150°C thermal perturbation, based on the mantle Vs-temperature relationship developed by Faul and Jackson (2005), and falls within the range imaged by both regional and global tomography models, which typically show shear wave speed reductions of 1–4% in this region (e.g., Porter et al., 2016; Brunsvick et al., 2024; Long, 2024). Such an anomaly may have contributed to recent

uplift in this part of North America (Fernandes et al., 2019), potentially shaping the Cenozoic tectono-thermal evolution of the Appalachian Mountains. The NAA may be linked to a slightly weaker anomaly ~650 km to the south, the Central Appalachian Anomaly (CAA) (Byrnes et al., 2019; Long et al., 2021), and whilst our primary focus is on the NAA, we evaluate this possibility. Edge-driven convection occurs where there is downwelling of asthenospheric mantle near lithospheric discontinuities (King and Anderson, 1998; King and Ritsema, 2000). However, as noted by Menke et al. (2016) and Carrero Mustelier and Menke (2021), upwelling beneath the NAA is unexpected and highly unusual given its location below the continental side of an ancient passive continental margin (Fig. 1B), which was presumably inactive since continental breakup along the Central Atlantic margins at ca. 183 Ma. Although near the Great Meteor hot spot track (see Tao et al., 2020), the NAA neither parallels it nor crosses the cratonic margin, suggesting these features are unrelated (Menke et al., 2016). The NAA lies beneath relatively thick lithosphere (100-150 km; Fig. 1B; Afonso et al., 2019), although it may locally be as thin as ~60-80 km (Espinal et al., 2024; Fig. S1 in the Supplemental Material). Nevertheless, some studies have questioned whether the lithosphere is thinned sufficiently to promote edge-driven convection (Carrero Mustelier and Menke, 2021). Farther seaward of the NAA, the lithosphere thickens to ~150 km for several hundred kilometers, with only a subtle thinning gradient seen at the COB (Fig. 1B). The NAA is thus enigmatic, leading to suggestions that it represents an unusual case of persistent, vigorous convection along the edges of the Laurentian craton (Menke et al., 2016; Brunsvik et al., 2024).

#### A ROLE FOR CONVECTIVE INSTABILITIES?

46

47

48

49

50

51

52

53

54

55

56

57

58

59

60

61

62

63

64

65

66

We examine whether the NAA represents a Rayleigh-Taylor instability, as proposed by Long et al. (2021) for the CAA, but suggest instead that the instability migrated over time along the

continental roots from a more distant, now-extinct rift system. We stress that this scenario complements—rather than replaces—earlier models, since all previous seismic observations of this feature remain valid and are simply interpreted in a new light.

69

70

71

72

73

74

75

76

77

78

79

80

81

82

83

84

85

86

87

88

89

90

91

Recent thermo-mechanical models have shown that continental rifting and breakup can generate a chain of Rayleigh-Taylor instabilities that propagates inboard of the rift over time (Gernon et al., 2023, 2024). These convective instabilities cause delamination by exploiting the density and strength contrast between the colder lithosphere and the hotter asthenosphere across the thermal boundary layer. This process bears similarities to small-scale convection and lithospheric dripping, which have been proposed as drivers of plateau uplift in eastern Anatolia (Göğüş and Pysklywec, 2018) and lithospheric erosion of the Wyoming craton (Dave and Li, 2016). However, in those cases, the mantle reorganization is linked to plate collisions, whereas in the NAA context, the convective instability may originate from rift-induced edge-driven convection. Specifically, the first delamination event occurs near the rift and is triggered by a perturbation of the lithospheric root by edge-driven convection, generating a family of sequential Rayleigh-Taylor instabilities that propagate inboard of the rift over time. Such instabilities migrate continentward at a rate of  $\sim 20 \pm 5$  km/Myr, removing the thermal boundary layer and driving adiabatic upwelling of convective mantle and kimberlite volcanism (in cratonic contexts; Gernon et al., 2023). Convective erosion of keels can promote isostatic uplift and denudation across 'stable' cratons, leading to the formation of elevated plateaus (Gernon et al., 2024).

A key aspect of this model is that convective instabilities may represent a legacy of continental rifting and breakup that persists in the mantle for many tens to over a hundred million years. A propagating instability could easily be misinterpreted as an isolated edge-driven convective cell, since at any given time it appears spatially fixed—and its occurrence along ancient

continental margins may be coincidental rather than causal. However, over geologic timescales, these chains of instabilities are dynamic and mobile, slowly and sequentially migrating along the continental root. A causal linkage with the Central Atlantic margin thus merits reconsideration.

### ATLANTIC RIFT SYSTEMS

The margins of the Central Atlantic rift system and its northern extension to the Labrador-Greenland Sea form a complex network of boundaries that were active at different times (Fig. 2), complicating the task of categorically tying instabilities to a single boundary. The North American continental margin commenced rifting at 240 Ma, with breakup occurring around 185–182 Ma (Brune et al., 2016). Meanwhile, the COB in the Labrador Sea is much younger, with rifting starting at ~120 Ma (but potentially as early as the late Jurassic; Dickie et al., 2011) and breakup occurring at 90–80 Ma, culminating at ca. 82 Ma (Fig. 2). Given the difficulties in associating the upwelling with the Central Atlantic COB—namely, its prolonged tectonic inactivity and the presence of relatively thick lithosphere (Carrero Mustelier and Menke, 2021)—we explore the alternative possibility that the feature represents a convective instability linked to the younger, more distal, Labrador Sea margins (Figs. 1-2).

A key characteristic supporting the identification of the NAA as a Rayleigh-Taylor instability is its length scale: the anomaly spans ~350–400 km in diameter (Menke et al., 2016), comparable to the predicted wavelength of such instabilities in geodynamic models, where upwellings are typically ~200 km wide (Fig. 3; Gernon et al., 2024). These features are marked by focused regions of upwelling and downwelling (Fig. 3), with the former capable of locally warming—and thermally eroding—the lithospheric keel. This behavior is consistent with previous interpretations of the NAA as a thermal upwelling and with its earlier diagnosis as an edge-driven

convection cell (King and Anderson, 1998; King and Ritsema, 2000)—a dynamically similar phenomenon.

#### **RESULTS & DISCUSSION**

To test a link between the NAA and distal rifting at the Labrador Sea, we measured its geospatial offset from the COB using QGIS (Fig. 1). The NAA lies ~1830–1880 km from the Labrador margin (Fig. 1; Fig. 4A). Assuming a propagation rate of 20 km/Myr—consistent with geodynamic models and kimberlite migration (Gernon et al., 2023)—this offset implies initiation at ca. 94–91 Ma (Fig. 4B), between rift onset and breakup, near the timing of rift acceleration (Brune et al., 2016) (Fig. 4D).

The propagation velocity of convective instabilities is controlled in part by activation energy and hence the viscosity used in geodynamic models. Previous work shows that plausible ranges in activation energy yield migration rates of 14–33 km/Myr (Gernon et al., 2023). The impact of this variability is to broaden the range of possible origination times for the initial instability. Using this range of migration rates and the full span of distances associated with the NAA (Fig. 4A), we conducted a Monte Carlo simulation (10,000 runs) employing beta distributions for both distance and rate. This yields a distribution of estimated origination times (Fig. 4C), with a median of 93.6 Ma and 10th and 90th percentiles of 75 Ma and 116 Ma, respectively. These results do not change our conclusion, as most estimates (~91%) fall within error of the rifting and breakup window when the initial instability forms (Fig. 4B), and even the lower bounds remain geologically plausible given the tectonic history of the margin.

The modeled migration characteristics of the NAA support its interpretation as a Rayleigh-Taylor instability that has sequentially propagated inboard of the Labrador Sea rift system over time. Numerical and analogue models show that delamination can evolve as drip-like features, which are influenced by lithospheric structure and strain localization (e.g., Elkins-Tanton, 2007). Thus, the stepped, irregular base of the adjacent North American craton likely shaped the geometry of the observed anomaly (Fig. 1). Seismic constraints offer supporting evidence (though not necessarily precluding edge-driven convection). Seismic tomography reveals low-velocity anomalies at 200 km depth (Fig. 1D) that are absent below 550 km (Schmandt and Lin, 2014), perhaps indicating a shallow mantle origin (cf. Fig. 3). In addition, SKS-splitting shows the anomaly is associated with both localized, low magnitude and NE-striking upper mantle anisotropy (Long, 2024), indicative of a combination of the vertical and SW directed mantle flow expected for a SW-migrating convective instability. While the ultimate causal mechanisms differ, our model (Fig. 3) complements the interpretation of the NAA as the upwelling limb of a small-scale convection cell (Menke et al., 2016). A distal origin help reconcile timing problems noted with the proximal edge-driven convection hypothesis (Carrero Mustelier and Menke, 2021), and the NAA's location hundreds of kilometers inboard of the Central Atlantic COB (Fig. 1B).

An outstanding question is whether the NAA could be linked to the CAA, the second largest seismic anomaly along the east coast (Figs. 1A, 1C; Fig. S2). Previously, the CAA has been attributed to lithospheric delamination followed by small-scale convection (Mazza et al., 2014; Byrnes et al., 2019). The CAA may represent one, or perhaps more, Rayleigh-Taylor instabilities (Long et al., 2021). Might this instability also be linked to rifting in the Labrador Sea? Applying the same analysis as before (Fig. 4A) would imply that the CAA originated ca. 135 to 120 Ma (Fig. 4B; Fig. S3), following the proposed timing of Labrador rift inception in the late Jurassic (Dickie et al., 2011). Thus, the CAA could represent an early instability associated with the development of a steep lithosphere-asthenosphere boundary gradient during early-stage rifting (cf. Gernon et al., 2023). Indeed, the CAA's inferred low degrees of melting (~1%) (Evans et al., 2019; Mittal et

al., 2023) closely match expectations for such instabilities based on hydrous decompressional melting models (Gernon et al., 2023). The CAA region's volcanic history suggests preconditioning to delamination-related melting (Mazza et al., 2014), likely augmented by hydrous phases that weaken the lithospheric keel and locally promote its removal (Evans et al., 2019).

Although the NAA may relate to Cenozoic Appalachian uplift (Fernandes et al., 2019), cold and dry climates and low erosion rates (~10 m/Myr; Hergarten and Kenkmann, 2019) suggest limited denudation over the past 30 Ma. Nonetheless, lithospheric delamination may have contributed to earlier topographic rejuvenation in the Central Appalachians (Miller et al., 2013). Should we expect to see remnants of earlier instabilities (i.e., weak anomalies) along the proposed path of this chain (Fig. 2)? Relatively sparce seismic coverage north of the NAA—particularly across Newfoundland, Labrador, and the Gulf of St. Lawrence—limits our ability to detect such anomalies. Even so, if earlier instabilities propagated in a stepwise manner every ~10 Myr, as seen in our geodynamic models (Gernon et al., 2023, 2024), their thermal signals would likely have been erased by conductive re-thickening of the thermal boundary layer over ≥10 Myr timescales (Yuan et al., 2017).

More speculatively, a pronounced ~200-km-wide seismic anomaly beneath north-central Greenland (Greve, 2019; Zhang et al., 2024, and references therein) conforms with the projected northward trajectory of the proposed NAA initiation site (Fig. 2), suggesting a possible shared origin. Applying the same geospatial analysis as before, the Greenland anomaly is projected to have formed at ~80 Ma, near coincident with breakup (Figs. 4B, 4D; Fig. S4). A model in which an instability arrived more recently may help reconcile the persistence of a thermal anomaly long after other contenders such as the Iceland plume at ~60 Ma (e.g., Martos et al., 2018) would likely

182 have dissipated through thermal advection and diffusion. This raises the intriguing possibility of a 183 unified mechanism linking the NAA, CAA, and Greenland anomalies. 184 185 **ACKNOWLEDGMENTS** 186 Seismic tomography sections were made using the SubMachine Engine developed by Kasra 187 Hosseini. We thank Joseph Byrnes and two anonymous reviewers for detailed reviews that greatly 188 improved the paper. Gernon was supported by the WoodNext Foundation (Texas, USA), a donor-189 advised fund program. 190 191 REFERENCES CITED 192 Afonso, J.C., Salajegheh, F., Szwillus, W., Ebbing, J., and Gaina, C., 2019, A global reference 193 model of the lithosphere and upper mantle from joint inversion and analysis of multiple 194 data sets: Geophysical Journal International, v. 217, p. 1602–1628. Doi: 195 10.1093/gji/ggz094. 196 Amaru, M. L., 2007, Global travel time tomography with 3-D reference models: Unpublished PhD 197 thesis. Utrecht University. 198 Brune, S., Williams, S., Butterworth, N, and Müller, R.D., 2016, Abrupt plate accelerations shape 199 rifted continental margins: Nature, v. 536, p. 201–204. Doi: 10.1038/nature18319. 200 Brunsvik, B., Eilon, Z., and Lynner, C., 2024, Plate-scale imaging of eastern US reveals ancient 201 and ongoing continental deformation: Geophysical Research Letters, v. 51, 202 e2024GL109041. Doi: 10.1029/2024GL109041.

Byrnes, J.S., Bezada, M., Long, M.D., and Benoit, M.H., 2019, Thin lithosphere beneath the

central Appalachian Mountains: Constraints from seismic attenuation beneath the MAGIC

203

- 205 Science Letters, v. 519, p. array: Earth and Planetary 297-307. Doi: 206 10.1016/j.epsl.2019.04.045. 207 Carrero Mustelier, E., and Menke, W., 2021, Seismic anomalies in the southeastern North 208 American asthenosphere as characterized with body wave travel times from high-quality 209 teleseisms: Tectonophysics, v. 809, 228853. Doi: 10.1016/j.tecto.2021.228853. 210 Dave, R., and Li, A., 2016, Destruction of the Wyoming craton: Seismic evidence and geodynamic 211 processes: Geology, v. 44, p. 883–886. Doi: 10.1130/G38147.1. 212 Dickie, K., Keen, C.E., Williams, G.L., and Dehler, S.A., 2011, Tectonostratigraphic evolution of 213 the Labrador margin, Atlantic Canada: Marine and Petroleum Geology, v. 28, p. 1663-214 1675. Doi: j.marpetgeo.2011.05.009. 215 Elkins-Tanton, L. T., 2007, Continental magmatism, volatile recycling, and a heterogeneous 216 mantle caused by lithospheric gravitational instabilities: J. Geophys. Res., v. 112, p. 217 B03405. Doi:10.1029/2005JB004072. 218 Espinal, K., Long, M. D., Karabinos, P., & Bourke, J. R., 2024, Lithospheric structure above the 219 Northern Appalachian Anomaly: Initial results from the NEST array: Geophysical 220 Research Letters, v. 51, e2024GL109955. Doi: 10.1029/2024GL109955. 221 Evans, R. R., Benoit, M. H., Long, M. D., Elsenbeck, J., Ford, H. A., Zhu, J., and Garcia, X., 2019, 222 Thin lithosphere beneath the Central Appalachian Mountains: A combined seismic and 223 magentotelluric study: Earth and Planetary Science Letters, v. 519, p. 308-316. Doi:
- Faul, U. H. and Jackson, I., 2005, The seismological signature of temperature and grain size variations in the upper mantle: Earth and Planetary Science Letters, v. 234(1-2), p. 119134.

10.1016/j.epsl.2019.04.46.

- Fernandes, V. M., Roberts, G. G., White, N., and Whittaker, A. C., 2019, Continental-scale
- landscape evolution: A history of North American topography: Journal of Geophysical
- 230 Research: Earth Surface, v. 124, p. 2689-2722. Doi: 10.1029/2018JF004979.
- Gernon, T.M., Jones, S.M., Brune, S., Hincks, T.K., Palmer, M.R., Schumacher, J.C., Primiceri,
- R.M., Field, M., Griffin, W.L., O'Reilly, S.Y., Keir, D., Spencer, C.J., Merdith, A., and
- Glerum, A., 2023, Rift-induced disruption of cratonic keels drives kimberlite volcanism:
- Nature, v. 620, p. 344–350. Doi: 10.1038/s41586-023-06193-3.
- Gernon, T.M., Hincks, T.K., Brune, S., Braun, J., Jones, S.M., Keir, D., Cunningham, A., and
- Glerum, A., 2024, Coevolution of craton margins and interiors during continental breakup:
- Nature, v. 632, p. 327–335. Doi: 10.1038/s41586-024-07717-1.
- Göğüş, O.H., and Pysklywec, R. N., 2008, Mantle lithosphere delamination driving plateau uplift
- and synconvergent extension in eastern Anatolia: Geology, v. 36; p. 723-726. Doi:
- 240 10.1130/G24982A.1.
- Greve, R., 2019, Geothermal heat flux distribution for the Greenland ice sheet, derived by
- combining a global representation and information from deep ice cores: Polar Data Journal,
- v. 3, p. 22–36. Doi: 10.20575/00000006.
- Hergarten, S. & Kenkmann, T., 2019, Long-term erosion rates as a function of climate derived
- from the impact crater inventory: Earth Surface Dynamics, v. 7, p. 459-473.
- 246 Doi:10.5194/esurf-7-459-2019.
- Hosseini, K., Matthews, K. J., Sigloch, K., Shephard, G. E., Domeier, M., & Tsekhmistrenko, M.,
- 248 2018, SubMachine: Web-based tools for exploring seismic tomography and other models
- of Earth's deep interior: Geochemistry, Geophysics, Geosystems, v. 19, p.1464–1483.
- 250 Doi:10.1029/2018GC007431.

- King, S. D., and Anderson, D. L., 1998, Edge-driven convection: Earth and Planetary Science
- 252 Letters, v. 160, p. 289–296, doi:10.1016/S0012-821X(98)00089-2.
- King, S. D., and Ritsema, J., 2000, African hot spot volcanism: Small-scale convection in the upper
- mantle beneath cratons: Science, v. 10, p. 1137–1140.
- 255 Doi:10.1126/science.290.5494.1137.
- 256 Long, M. D., Wagner, L. S., King, S. D., Evans, R. L., Mazza, S. E., Byrnes, J. S., et al., 2021,
- Evaluating models for lithospheric loss and intraplate volcanism beneath the Central
- Appalachian Mountains: Journal of Geophysical Research: Solid Earth, v. 126, p.
- 259 e2021JB022571. Doi: 10.1029/2021JB022571.
- Long, M. D., 2024, Evolution, Modification, and Deformation of Continental Lithosphere: Insights
- from the Eastern Margin of North America: Annual Review of Earth and Planetary Science,
- v. 52, p. 549-580. Doi: 10.1146/annurev-earth-040522-115229.
- Martos, Y., Jordan, T., Catalán, M., Jordan, T., Bamber, J., and Vaughan, D., 2018, Geothermal
- heat flux reveals the Iceland hotspot track underneath: Greenland, Geophys. Res. Lett., v.
- 265 45, p. 8214–8222. Doi: 10.1029/2018GL078289.
- Mazza, S.E., Gazel, E., Johnson, E.A., Kunk, M.J., McAleer, R., Spotila, J.A., Coleman, D. S.,
- 2014, Volcanoes of the passive margin: the youngest magmatic event in eastern North
- 268 America: Geology, v. 42, p. 483–486. <u>Doi: 10.1130/G35407.1</u>.
- Menke, W., Skryzalin, P., Levin, V., Harper, T., Darbyshire, F., and Dong, T., 2016, The Northern
- Appalachian Anomaly: a modern asthenospheric upwelling: Geophysical Research Letters,
- 271 v. 43, p. 173–10,179. Doi: 10.1002/2016GL070918.
- 272 Miller, S.R., Sak P.B., Kirby, E., and Bierman, P.R., 2013, Neogene rejuvenation of central
- Appalachian topography: Evidence for differential rock uplift from stream profiles and

- erosion rates: Earth and Planetary Science Letters, v. 369-370, p. 1-12. Doi:
- 275 10.1016/j.epsl.2013.04.007.
- 276 Mittal, V., Long, M. D., Evans, R. L., Byrnes, J. S., & Bezada, M., 2023, Joint analysis of seismic
- and electrical observables beneath the Central Appalachians requires partial melt in the
- upper mantle: Geochemistry, Geophysics, Geosystems, v. 24, e2022GC010690. Doi:
- 279 10.1029/2022GC010690.
- Müller, R. D., Zahirovic, S., Williams, S. E., Cannon, J., Seton, M., Bower, D. J., Tetley, M.G.,
- Heine, C., Le Breton, E., Liu, S., Russell, S.H.J., Yang, T., Leonard, J., and Gurnis, M.,
- 282 2019, A global plate model including lithospheric deformation along major rifts and
- orogens since the Triassic: Tectonics, v. 38, p. 1884–1907. Doi: 10.1029/2018TC005462.
- Pollitz, F. F., and W. D. Mooney, 2016, Seismic velocity structure of the crust and shallow mantle
- of the Central and Eastern United States by seismic surface wave imaging: Geophysical
- 286 Research Letters, v. 43, p. 118–126. Doi:10.1002/2015GL066637.
- Porter, R., Liu, Y., and Holt, W.E., 2016, Lithospheric records of orogeny within the continental
- US: Geophysical Research Letters, v. 43(1), p. 144-153.
- Schmandt, B., and Lin, F.-C., 2014, P and S wave tomography of the mantle beneath the United
- 290 States: Geophysical Research Letters, v. 41, p. 6342–6349. Doi: 10.1002/2014GL061231.
- 291 Tao, Z., Li, A., and Fischer, K. M., 2020, Hotspot signatures at the North American passive
- 292 margin: Geology, v. 49(5), p. 6–530. Doi: 10.1130/g47994.1
- Yuan, X., Heit, B., Brune, S., Steinberger, B., Geissler, W. H., Jokat, W., and Weber, M., 2017,
- Seismic structure of the lithosphere beneath NW Namibia: Impact of the Tristan da Cunha
- 295 mantle plume: Geochem. Geophys. Geosyst., v. 18, p. 125–141.
- 296 Doi:10.1002/2016GC006645.

Zhang, T., Colgan, W., Wansing, A., Løkkegaard, A., Leguy, G., Lipscomb, W., & Xiao, C., 2024, Evaluating different geothermal heat flow maps as basal boundary conditions during spin up of the Greenland ice sheet: The Cryosphere, v. 18 (1), p. 387-402. Doi: 10.5194/tc-18-387-2024.

### FIGURE CAPTIONS

**Figure 1**. (**A**) Map of North America (yellow box in global inset map) showing modelled locations of the NAA and CAA (Schmandt and Lin, 2014; Pollitz and Mooney, 2016; Menke et al., 2016; Long et al., 2021) relative to COBs (from Müller et al., 2019); red lines show mapped faults from the USGS's Geologic Map of North America (https://ngmdb.usgs.gov/gmna/); (**B**–**C**) Crosssections (see A for lines of section) traversing the NAA and CAA using the LithoRef18 global reference model (Afonso et al., 2019) (see Figs. S1-S2 for other thickness models); (**D**) Seismic tomography depth slice at 200 km beneath eastern North America (red box in global inset map), averaged across 16 models, extracted using SubMachine (Hosseini et al., 2018). (**E**) Seismic tomography cross-section (see A) based on the UU-P07 global model (Amaru, 2007).

**Figure 2**: Simplified plate tectonic reconstruction from GPlates (https://www.gplates.org/) showing the Labrador Sea rift at the point of breakup at ~80 Ma. Also shown is the projected track of the chain of convective instabilities. Inset shows extension velocity along the Labrador Sea Margins, from Brune et al. (2016).

**Figure 3**: Geodynamic model showing Rayleigh-Taylor instability formation beneath continental lithosphere (model from Gernon et al. (2024)). Note the convective removal of the lowermost

lithosphere shown in beige, which is associated with downwelling. This is accompanied by adiabatic upwelling of hotter asthenosphere, warming, and further thinning of the continental keel. EDC: edge-driven convection.

**Figure 4**: Spatial characteristics of the Northern and Central Appalachian Anomalies and the modeled initiation time of Rayleigh-Taylor instabilities. (**A**) Distance of the NAA and CAA from the Labrador Sea COB (n=1000 for each), for four seismic models (labeled). (**B**) Boxplot showing projected timing of initiation of the NAA/CAA and north-central Greenland anomaly (see Fig. S4), using the measured distances, and a migration rate of 20 km/Myr. (**C**) Density plot of modelled origination times for the initial NAA instability, generated using a Monte Carlo simulation (10,000 runs) with the observed distance of the NAA from the Labrador COB (Fig. 4A) and the likely range of migration rates (14–33 km/Myr) (the same analysis is repeated for CAA in Fig. S3). (**D**) Inferred migration rates of instabilities at probable inception points (i.e., rift onset, acceleration [ra], and breakup), alongside constraints from kimberlites (Gernon et al., 2023), including migration rates gleaned from geologic observations and analytical/geodynamic models.

# 336 Figure 1

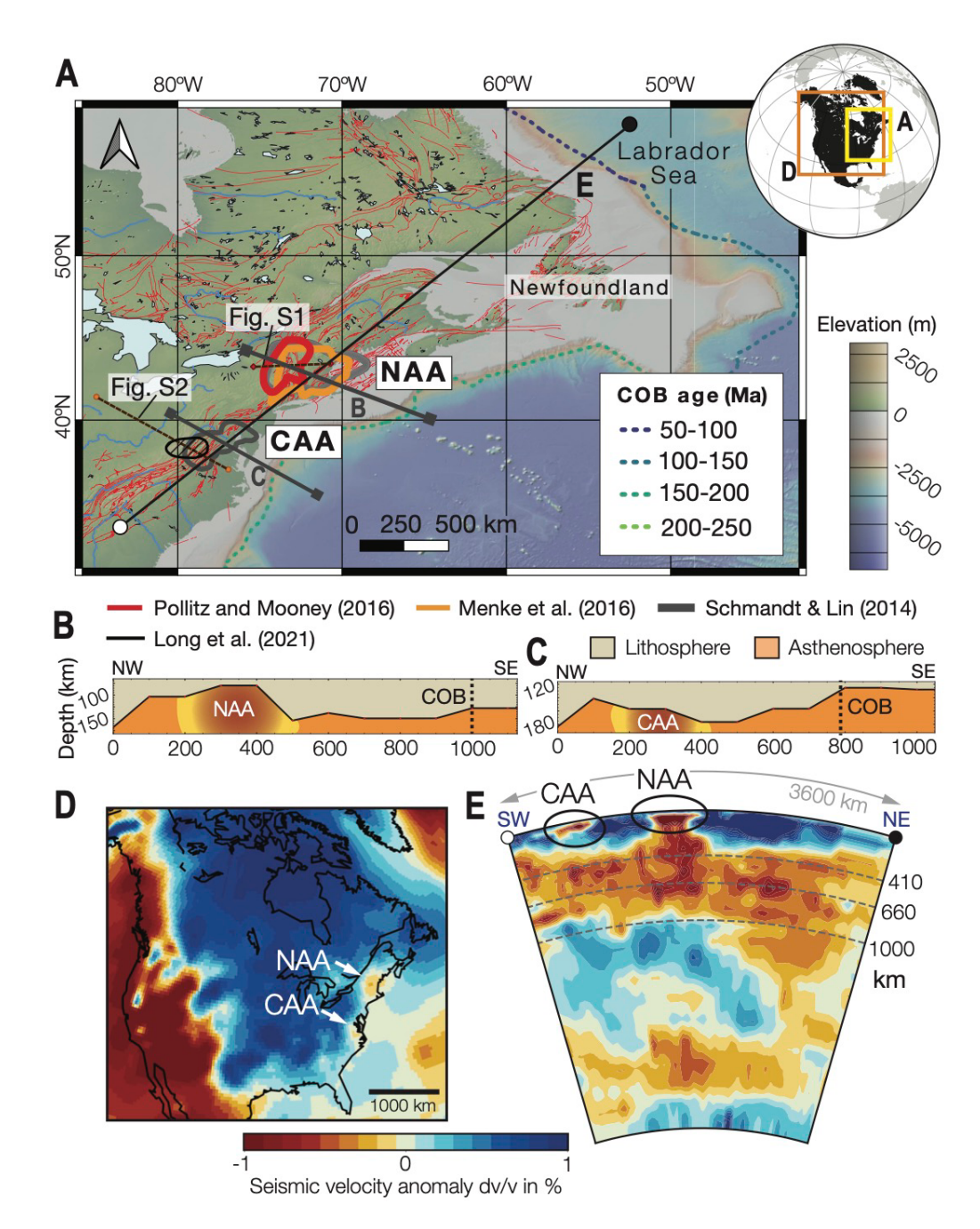
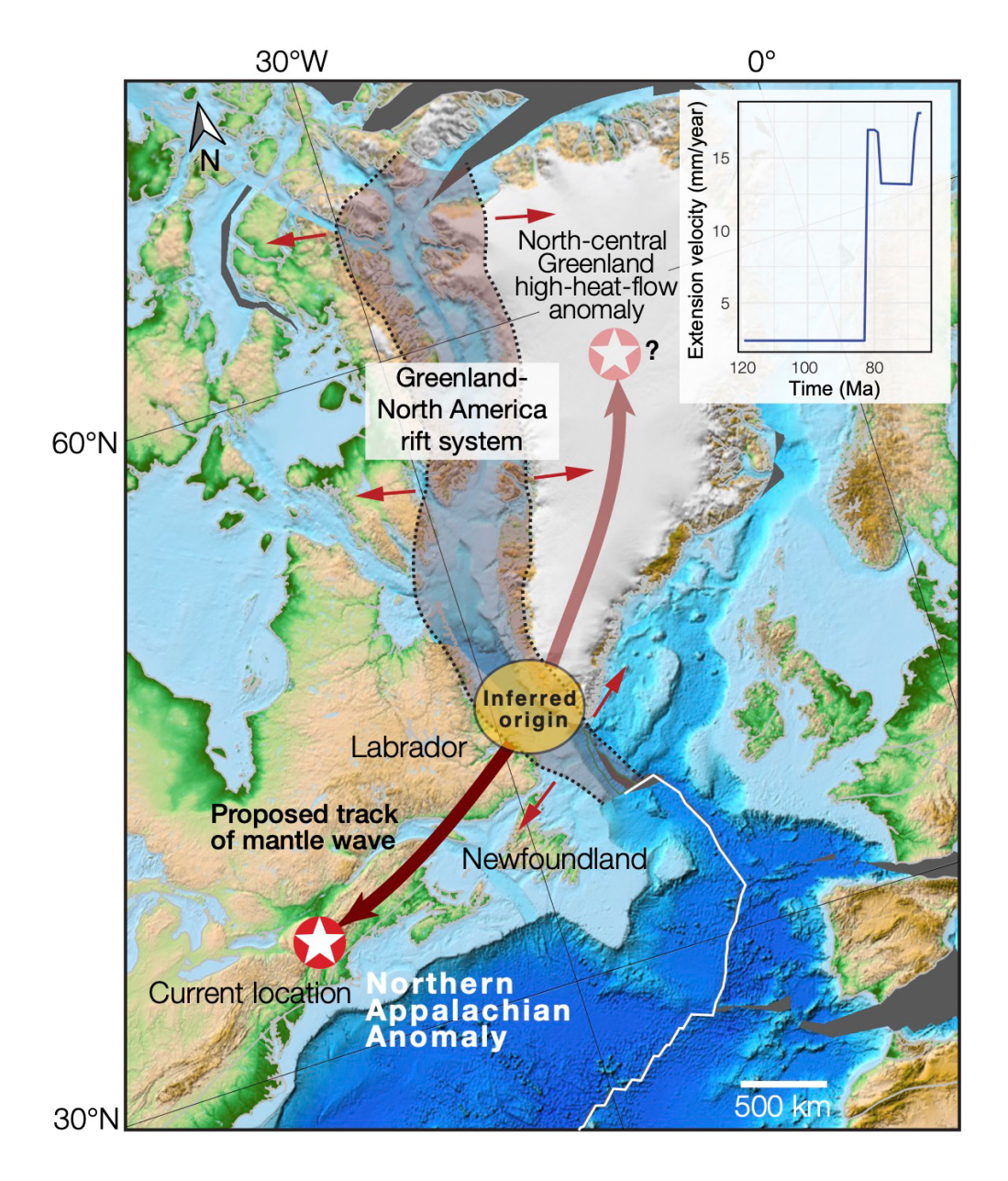


# **Figure 2**



340 Figure 3341

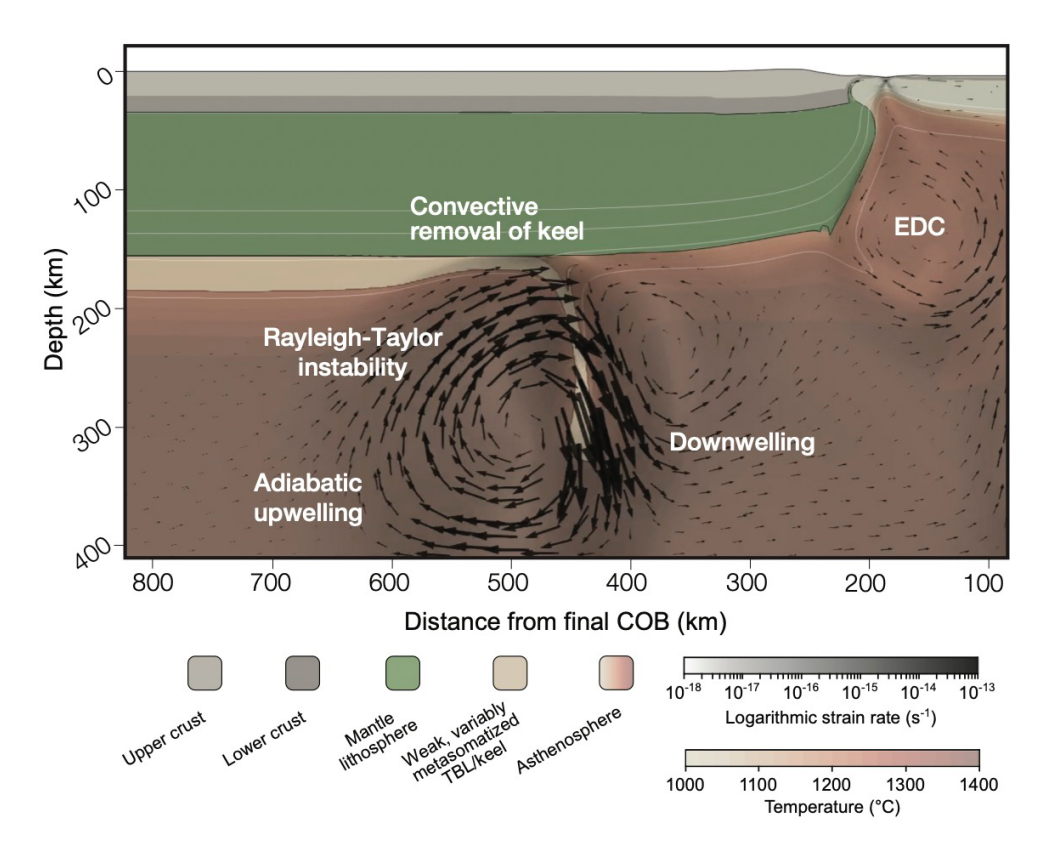
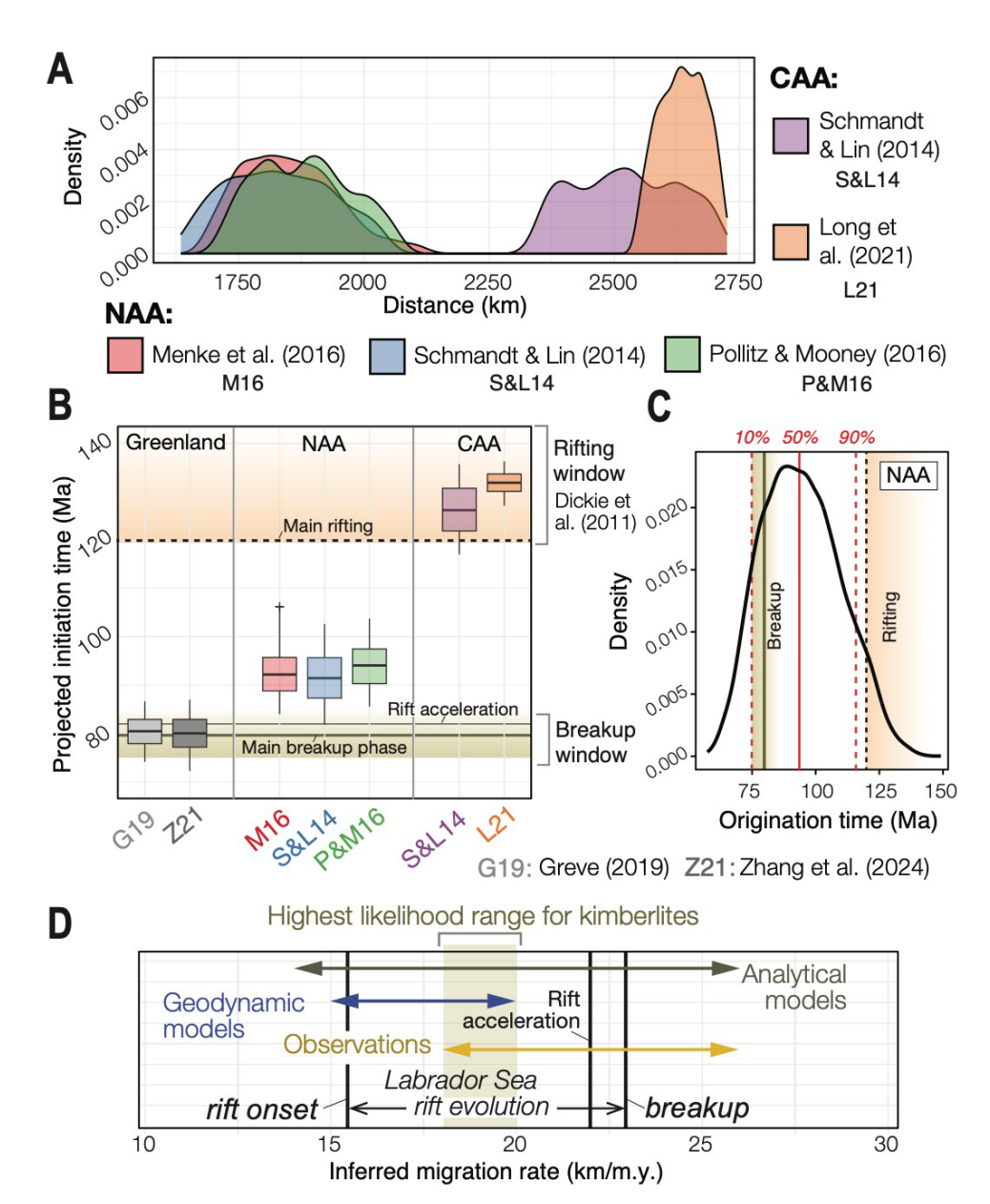


# **Figure 4**



### **Supplementary Figures**

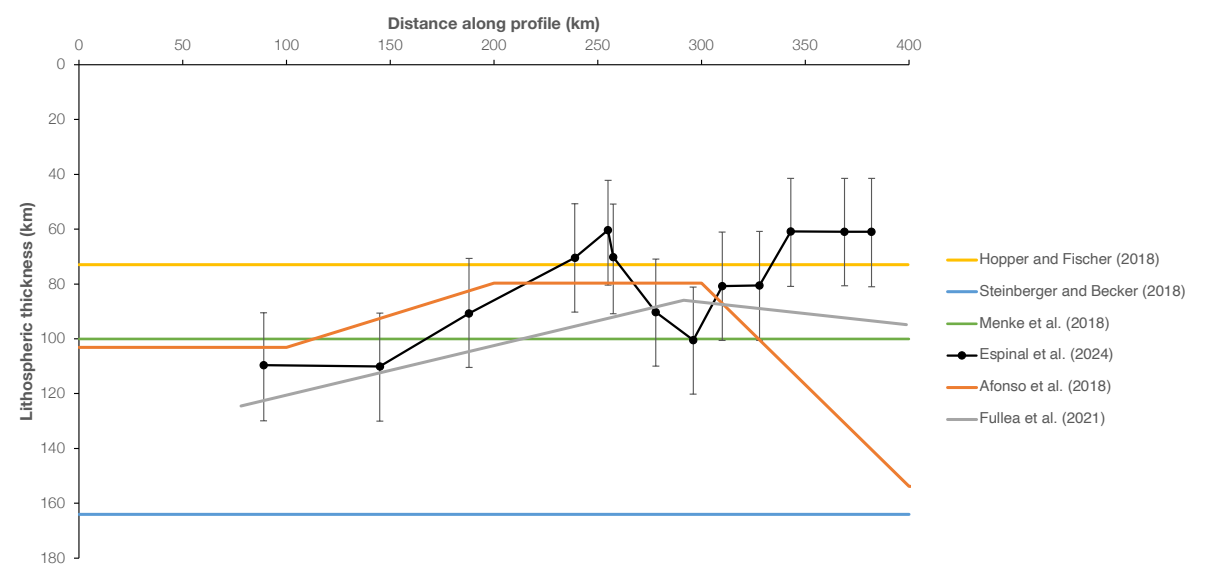


**Figure S1**: Alternative lithospheric thickness models across the Northern Appalachian Anomaly (for line of profile, see Fig. 1A). The models are from Hopper and Fischer (2018), Steinberger and Becker (2018), Menke et al. (2018), Espinal et al. (2024), Afonso et al. (2018) and Fullea et al. (2021). References not provided in the manuscript are given below.

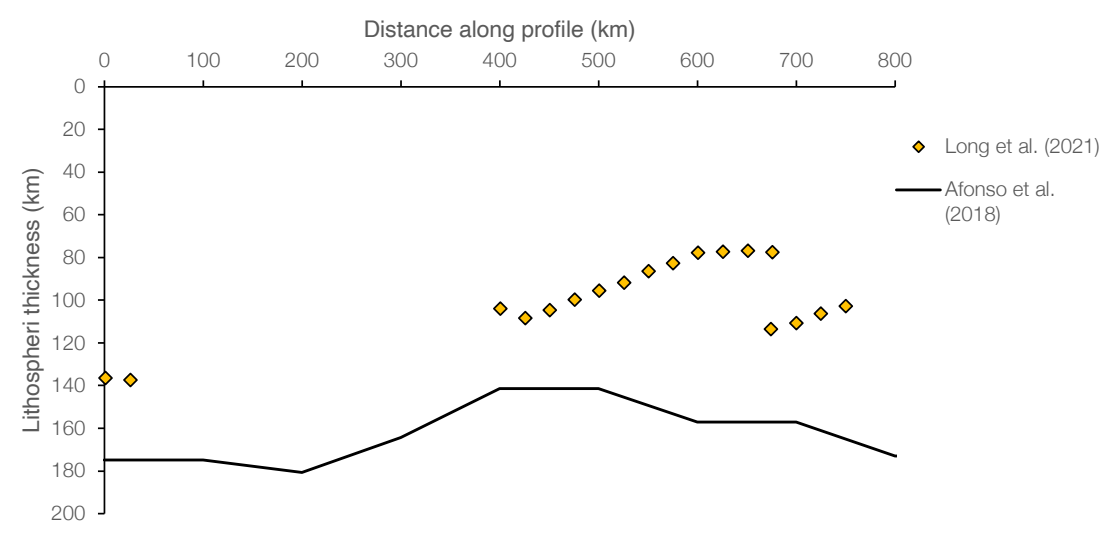


**Figure S2**: Lithospheric thickness models across the Central Appalachian Anomaly (for line of profile, see Fig. 1A). The black line shows the LithoRef18 model of Afonso et al. (2018). The yellow diamonds are interfaces that have been interpreted to represent the lithosphere-asthenosphere boundary (Long et al., 2021).

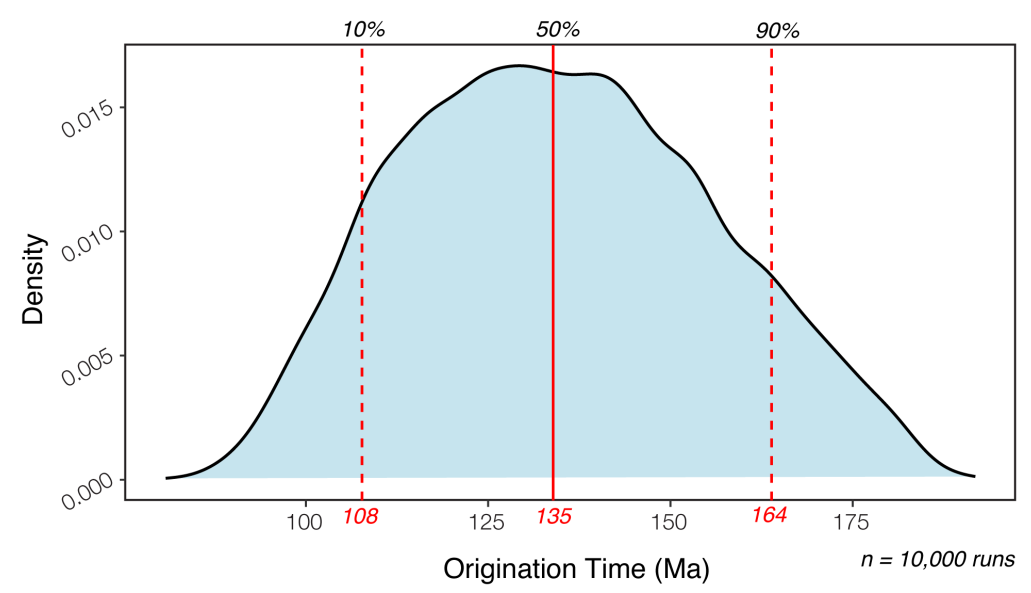


**Figure S3**: Density plot of modelled origination times for the proposed initial instability, generated using a Monte Carlo simulation (10,000 runs) with beta distributions applied to both the observed distance of the Central Appalachian Anomaly (using the mapped extent of Long et al., 2021; see Fig. 1A) from the Labrador continent—ocean boundary (i.e., ranging from 2542 to 2725 km; Fig. 4A). The migration rate is sampled from a beta distribution with the following properties (in km/m.y.): min=14, max=33, mean=20, variance=10.

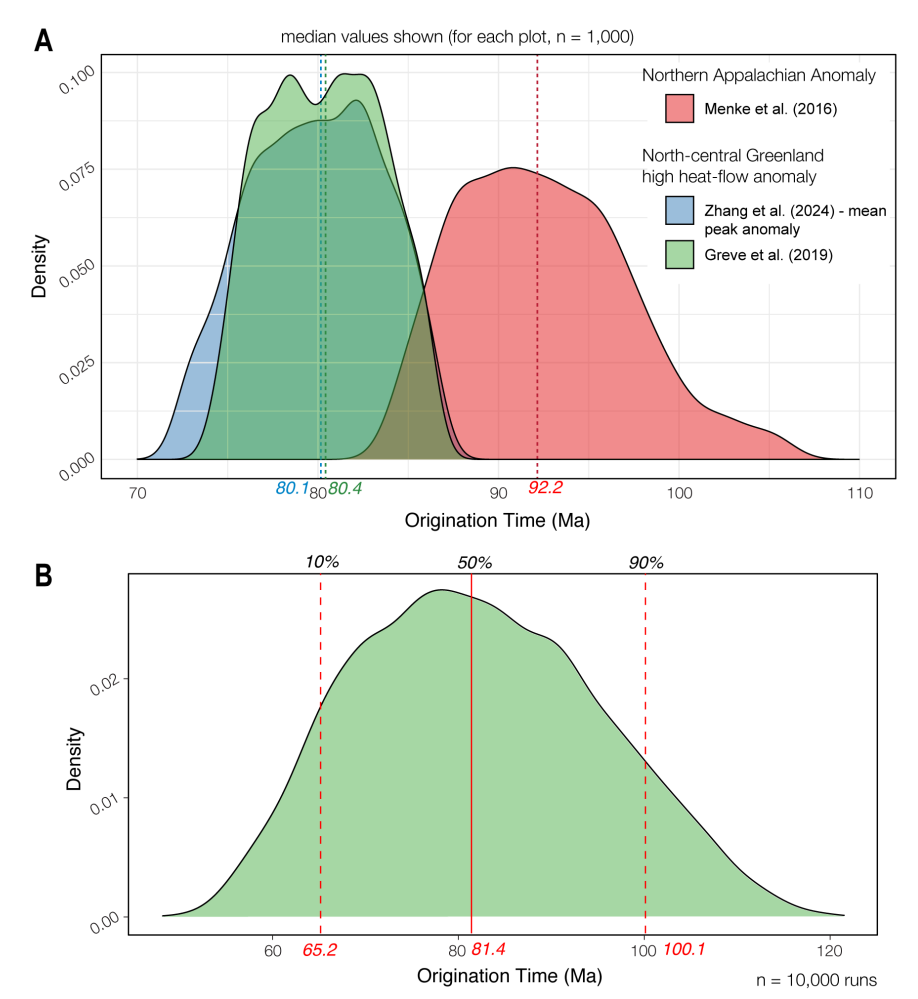


**Figure S4**: (A) Density plots showing the distribution of inferred origination ages for rift-related Rayleigh-Taylor instabilities, calculated based on the present-day locations of thermal anomalies including the NAA (Menke et al., 2016) and north-central Greenland (Greve et al., 2019; Zhang et al., 2024), relative to the southwestern Greenland margin—conjugate to the Labrador margin—and assuming a lateral migration rate of 20 km/m.y. Each plot represents results from n=1,000 randomly distributed points within a polygon representing the shape of the anomaly. For Zhang et al. (2024), this polygon represents the peak anomaly of the ensemble mean of seven heat flow models. Median inferred ages for the Greenland anomalies for two alternative heat-flow models are both approximately 80 Ma, closely corresponding to the timing of continental breakup (Fig. 4). (B) The sensitivity of the above estimates to variations in mantle viscosity (thus migration rate) for the example of the thermal anomaly of Greve (2019). The density plot was generated using a Monte Carlo simulation (10,000 runs), sampling from the observed distances of 1,000 random points within a polygon shapefile of the anomaly, from the southern Greenland (Labrador conjugate) continent—ocean boundary (i.e., 1482 to 1732 km). The migration rate is sampled from a beta distribution with the following properties (in km/m.y.): min=14, max=33, mean=20, variance=10.

### **Supplementary References**

Fullea, J., Lebedev, S., Martinec, Z., and Celli, N. L., 2021, WINTERC-G: Mapping the upper mantle thermochemical heterogeneity from coupled geophysical–petrological inversion of seismic waveforms, heat flow, surface elevation and gravity satellite data: Geophysical Journal International, v. 226(1), p. 146–191. Doi: 10.1093/gji/ggab094.

388	Hopper, E., and Fischer, K. M., 2018, The changing face of the lithosphere-asthenosphere boundary:
389	Imaging continental scale patterns in upper mantle structure across the contiguous U.S. With Sp
390	converted waves: Geochemistry, Geophysics, Geosystems, v. 19(8), p. 2593-2614. Doi:
391	10.1029/2018GC007476.

- Menke, W., Lamoureux, J., Abbott, D., Hopper, E., Hutson, D., and Marrero, A., 2018, Crustal heating and lithospheric alteration and erosion associated with asthenospheric upwelling beneath southern New England (USA): Journal of Geophysical Research: Solid Earth, v. 123(10), p. 8995–9008. Doi: 10.1029/2018JB015921.
- Steinberger, B., and Becker, T. W., 2018, A comparison of lithospheric thickness models: Tectonophysics, v. 746, p. 325–338. Doi: 10.1016/j.tecto.2016.08.001.